Article:
Michalchuk, A.A.L., Fincham, P.T., Portius, P. orcid.org/0000-0001-8133-8860 et al. (2 more authors) (2018) A Pathway to the Athermal Impact Initiation of Energetic Azides. Journal of Physical Chemistry C. ISSN 1932-7447

https://doi.org/10.1021/acs.jpcc.8b05285

A Pathway to the Athermal Impact Initiation of Energetic Azides.

Adam A.L. Michalchuk,[1,2] Peter T. Fincham,[3] Peter Portius,[4] Colin R. Pulham[1,2] and Carole A. Morrison[1*]

[1]EaStChem School of Chemistry and Centre for Science at Extreme Conditions, University of Edinburgh, Edinburgh, EH9 3FJ, UK.

[2]EPSRC Centre for Continuous Manufacturing and Crystallisation (CMAC), United Kingdom

[3]Defence Science and Technology Laboratory (DSTL), Porton Down, Salisbury, Wiltshire, SP4 0JG, UK.

[4] Department of Chemistry, University of Sheffield, Western Bank, Sheffield, S3 7HF, UK

ABSTRACT: Energetic materials (explosives, propellants and pyrotechnics) are used in a broad range of public and private sector applications. The design of novel, safe materials is therefore of critical importance. At present, physical mechanisms able to rationalize the impact sensitivity properties of energetic materials remain limited. Investigation therefore has required lengthy synthesis and experimental testing. Based on knowledge of the effects of mechanical impact, an *ab initio* model is developed to rationalize and describe the impact sensitivity of a series of crystalline energetic azide materials. It is found that electronic excitation of the azido anion is sufficient to permit bond rupture, and therefore offers a plausible mechanism for initiation of these materials. The athermal excitation can be achieved through consideration of non-adiabatic vibronic processes. Across the series of azides studied here, the electronic structure of the azido anion is found to remain largely constant. By considering only the relative rates of vibrational energy transfer within the crystalline materials it is found that a direct correlation exists between the relative impact sensitivity and the rate of energy up-conversion. Thus, the present contribution demonstrates a fully *ab initio* method to describe the athermal initiation of ideal, crystalline energetic materials, and predict their relative sensitivity. Without the need for any experimental input beyond a crystal structure, this method therefore offers a means to selectively design novel materials for targeted application.

Introduction

Energetic materials (explosives, propellants and pyrotechnics) span a broad range of applications. For example, silver fulminate is the explosive commonly used in household Christmas crackers, and nitroguanidine and potassium nitrate are propellants used in airbags and fireworks, respectively. Other well-known energetic materials such as 1,3,5,7-tetranitro-1,3,5,7-tetrazocane (HMX), 2,4,6-trinitrotoluene (TNT) and triamino-trinitro-benzene (TATB) find various defence and industrial applications. With use spanning a range of sectors, safety of these materials is of fundamental concern. A particularly critical parameter is the propensity of an energetic material to initiate on mechanical impact. The amount of impact energy required to induce initiation can vary enormously, leading to the classification of high explosives as primary (highly sensitive) or secondary (low sensitivity).[1] The former class, to which tri-acetone-tri-peroxide (TATP) belongs, can generally be initiated by very low mechanical impact. Secondary energetics, such as FOX-7, nitrotriazolone (NTO) or TATB, require higher input energies and are often detonated by the shock wave of a primary energetic material.[2] Tuning sensitivity properties is now a pressing area of research, with large screenings of novel molecules, crystal phases (polymorphs)[3–5] and multi-component materials (co-crystals and salts)[6–9] being conducted. At present the development of novel energetic materials requires production and experimental testing, with *a posteriori* rationalization of its properties. This method poses considerable safety hazards, yields limited fundamental understanding of structure/property relationships, and does not permit the targeted design of novel materials with tailored properties.

Considerable effort has been devoted to establishing correlations between a variety of physical and thermodynamic parameters with sensitivity.[10–13] Most commonly these been based on empirical relationships[14,15] such as oxygen balance[16] and electrostatic potential or charge density distribution.[17,18] In addition, numerous reports relate bond distances[19] and *ab initio* consideration of covalent bond dissociation energies[17,20,21] with sensitivities. Recent semi-empirical models based on covalent bond dissociation energies have proven to be very promising for predicting sensitivity.[22]

While these methods have been promising to varying degrees, the focus on isolated molecules does not account for the known differences in sensitivity between

polymorphic forms of energetic materials,[23] for differences that result by formation of multi-component energetic compounds, in which the same explosophore is present.[24] The need to consider condensed matter properties has been noted by various authors. This has led to attempts to relate a variety of crystalline properties with impact sensitivity, most notably intermolecular bond structure and packing,[25,26] packing density and volume,[27–29] ionisation potentials,[19] lattice energies,[19] deformation potentials,[26] electronic band gaps,[30,31] and most recently impact pressure-induced metallization.[32] In many cases, attempts at correlating such properties with impact sensitivity have proved to be promising from an empirical perspective, but a physical basis or rationale is often missing, which restricts their predictive power to within individual families of related compounds.[33] Some reports, however, have identified the importance of vibrational structure in predicting impact sensitivity,[34–39] which does offer potential for a more fundamental mechanism for impact sensitivity. These vibration-based models are based on the concept of vibrational up-pumping,[40,41] and both experimental[37] and theoretical models[39] of this kind have been proposed.

A particularly intriguing and broad class of energetic compounds are the azides, with examples derived from elements from across the periodic table. Despite the apparent chemical simplicity of these materials, a wealth of structural chemistry is present, with examples of molecular, polymeric and ionic crystal structures reported, alongside rich polymorphism.[42,43] Their initiation mechanism has been researched for nearly three-quarters of a century.[44] Some azides, such as NaN_3, display extremely low sensitivity, and have therefore found use in commercial applications. Others, such as $Cu(N_3)_2$, are so sensitive that they cannot be used for any practical application. With such wide-spanning physical properties there is much interest in their continued development as novel energetic materials.[45]

The breadth of initiation energies displayed by the simple inorganic azides is astonishing. The typical rationales of bond dissociation energies no longer apply, given that the energetic molecule, the azide anion, is the same in each case. A physical basis for this phenomenon has not yet been elucidated, although some qualitative trends, including bond lengths, cation ionization potentials and symmetry breaking of azide vibrational modes have been noted.[19,46] More physical models have also been proposed, noting that crack propagation rates may be linked to sensitivity.[47] However, no unified mechanism has yet been proposed to explain the sensitivity relationships observed for these compounds.

Two general mechanisms have been postulated for the impact-induced initiation of energetic materials. In the first, impact induces localized buildup of heat (hot spots), which ultimately leads to a thermally induced initiation event in the vicinity of the hot spot.[48] The second mechanism relates to the direct transfer of energy from the impact shock wave into the structure of the material, often by fracture processes. These two models describe the thermal and athermal modes, respectively.

In the present contribution a fully *ab initio* approach is employed to develop a fundamental physical mechanism to describe the athermal initiation mechanism in energetic materials. This work provides a new fundamental mechanism to describe and rationalize the impact sensitivity of energetic azide compounds. By establishing a physical mechanism for impact-induced initiation, we move towards the capacity to design *in silico* novel materials for specific applications.

General Theory

To begin to understand the mechanism by which a mechanical impact can elicit a chemical response, we must consider the physical effects of the impact itself. On impact, two main processes occur within the impacted body: (1) dynamic compression and (2) fracture of the crystal surface layers.[49] In the first, a compressive shock wave passes through the material, akin to an acoustic wave. This dynamic compression has been suggested to lead to vibrational excitation of the lattice by a two-fold mechanism.[50] First, the increase in pressure leads to a shift in the vibrational frequencies of the material, which is then followed by a temperature effect. For the adiabatic compression of a solid,[51]

$$\left(\frac{T}{T_o}\right) = \left(\frac{V}{V_o}\right)^{-\Gamma} \qquad \text{Equation 1}$$

where Γ is the Grüneisen parameter (and V, T represent volume and temperature). The exact achievable temperature upon compression depends largely on the heat capacity of the material.[40] The excitation process therefore depends greatly on pressure and temperature.[52–54] Early work has suggested that for a typical organic material such as naphthalene, a modest shock (4 GPa) is associated with a total increase in internal energy of 37 000 cm^{-1}, which is distributed between heat and work.[40] This energy remains localized in the lattice phonon bath, in conjunction with the progression of the shock front.[52,53,55] For the system studied, this led to an initial phonon vibrational quasi-temperature of 2300 K, with the overall vibrational quasi-temperature remaining equilibrated to ambient conditions.[40]

The second process, fracture, is well described within the theories of tribophysics and the Hertzian theory of contact stresses.[49] Within the contact surface, stresses build beyond the elastic limit of the material. This leads to plastic deformation in the form of dislocations, or fracture.[47] It has been suggested that, analogous to the rupture of a loaded spring, the sudden rupture of non-covalent interactions leads to rapid excitation of lattice vibrations associated with the ruptured interaction.[37]

In both cases, the mechanical impact leads to rapid vibrational excitation of the low frequency lattice vibrational modes. Within an anharmonic lattice, this

excess energy rapidly equilibrates. Due to the large anharmonicity of the lattice vibrational modes, equilibration within the delocalized phonon modes occurs quickly,[56,57] reaching a quasi-equilibrium state of a vibrationally 'hot' phonon region, or *bath*. This phonon bath has an upper bound value, defined as Ω_{max}, Figure 1. The remaining vibrational space is vibrationally 'cold'. Following rapid equilibration of the phonon bath, vibrational energy continues to scatter upwards. The general process of up-conversion occurs in two stages. First, phonon scattering of the phonon bath modes leads to excitation of an intermediate librational mode, a *doorway mode*,[56] which can subsequently scatter with another doorway mode, or with other phonon bath modes to reach higher-lying internal molecular vibrational modes, Figure 1. We note that this total vibrational equilibration process has been found to occur more rapidly than thermally-induced chemical decomposition,[55] with previous works suggesting vibrational up-conversion occurs on the order of a few picoseconds, and occurs more rapidly around defects.[40,58]

To achieve a chemical response, the vibrational energy must finally reach a particular molecular vibrational mode, the *target mode*. Vibrationally exciting this mode reduces the energy separation of the frontier orbitals, such that athermal bond rupture (through non-adiabatic processes) follows.[59–61] For the case of energetic materials, this bond rupture is responsible for initiation of a cascade of reactions, ultimately leading to an explosion. Typically, this is likely to involve rupture of a N-N or C-N bond. Thus the target frequency can generally be thought to include deformation of these bonds. However, the exact target mode cannot be known without thorough investigation. Indeed, McNesby states the importance of transferring the phonon bath energy to the 'internal vibrational manifold', which is set by a lower limit cutoff of 200 cm^{-1} (denoting the top of the phonon bath, Ω_{max}) and an upper cutoff of 700 cm^{-1}.[37] However, the relative structural simplicity of the azide compounds studied in this work should permit the actual target frequencies within this manifold to be identified. Likewise, the value of Ω_{max}, and the presence of any doorway modes, will also be system dependent. All of these features can be obtained from first principles simulation. With data obtained in this way, mode coupling pathways required for up-conversion to the target mode can be examined. The number of up-conversion pathways directly links to the ease of energy transfer to the target mode, and thus the likelihood of subsequent vibronic processes. It therefore becomes worthwhile to seek a correlation between the likelihood of vibrational up-conversion with measured impact sensitivities for the azide series of compounds.

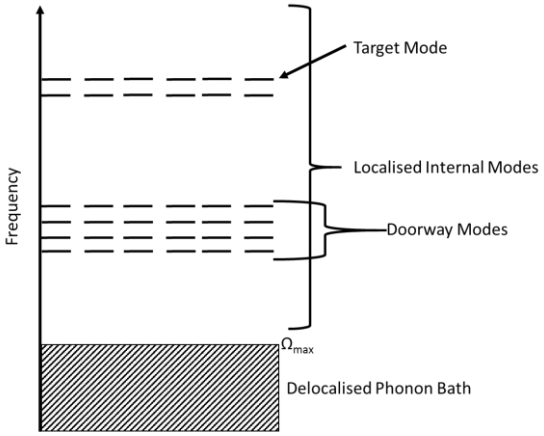

Fig 1: Schematic representation of the vibrational energy ladder traversed by mechanical (shock) impact energy. Injected energy begins in the delocalized phonon bath, up-converting to the localized molecular-based target modes *via* intermediate doorway modes.

Computational Methods

Gas phase calculations. Calculations of isolated molecules were performed *in vacuo* using Molpro 2012.[62] Geometry optimization and subsequent vibrational frequency calculation was performed to ensure equilibrium geometry was obtained. The electronic structure was built upon a CAS(8,8)/6-31+G* calculation, on which a MRCI calculation was added for the same active space and basis set. Spin orbit coupling was calculated using the same approach, based on the MRCI transition integrals and the 2nd order Douglas-Kroll operators.

Condensed Matter Calculations. All input unit cells were taken from experimentally determined structures, deposited in the Inorganic Crystal Structural Database (ICSD, FIZ Karlsruhe), with compound-specific information available in the ESI, S1. Structures were fully relaxed to ensure minimization of all forces within the system. Full details of the relaxation criteria are given in the ESI S1. We note that all calculations were performed using dispersion correction. All plane-wave (PW) based electronic structure calculations were performed using QuantumEspresso v6.1.[63] Electronic band structures were generated using the GGA functional of Perdew-Burke-Ernzerhof (PBE).[64] The band structures were generated along high symmetry paths. Crystal Overlap Hamilton Populations were then obtained using the LOBSTER implementation for Quantum Espresso.[65] Note as GGA based band gaps are known to provide poor agreement with experiment, further band structures were generated in CRYSTAL17[66] using the HSE06[67] hybrid DFT functional, which has been demonstrated to offer reasonable agreement with experimental band gaps for a broad range of materials.[68] Those presented here can therefore be regarded as accurate to within a reasonable level of confidence. Convergence criteria and basis sets can be found in ESI S2. The HSE06 functional was also used to calculate the 'band gap' of an isolated azido anion

molecule, which was placed in a periodic boundary condition box of 10 Å^3. A background Coulombic potential was added to ensure net charge neutrality.

Full phonon band structure calculations were performed in Quantum Espresso v6.1 and CASTEP v16.[69,70] Details of individual sampling is given in the ESI S3, including the selected dispersion correction scheme. In all cases, the dynamical matrix was evaluated on a coarse grid, followed by Fourier interpolation to a finer grid in *k*-space. The acoustic sum rule was implemented in reciprocal space. For the purpose of the present study, LO-TO splitting was explicitly removed, ensuring all dispersion plots represent the underlying physical structure of the material.

Results and Discussion

In order to build a model for the impact sensitivity of crystalline energetic azides, a test set was constructed (Table 1) that encompassed a wide range of reported experimental sensitivities and covered a breadth of structural types, including ionic, polymeric and molecular. Two of the selected materials are based on molecular cationic species: triaminoguananidinium azide (TAGZ) and ammonium azide (NH_4N_3). We note that experimental measurement of energetic material sensitivity can be unreliable, and that the literature is ripe with conflicting reports based on variations in sensitivity resulting from particle size, impurities, crystal defects and inconsistencies in experimental conditions.[63] In the present work, the model is based on ideal, crystalline materials and is therefore not met with such issues. The results presented herein can therefore be taken as the intrinsic sensitivity of the pure crystalline state. In terms of the present materials, literature discrepancies are particularly prevalent for the ordering of the sensitive materials listed in Table 1. The sensitivity classifications are based on the following: (1) $Ba(N_3)_2$, is quoted by some as being more sensitive than AgN_3,[19] and by others as less sensitive.[72] Its impact sensitivity (energy at which a sample has a 50% probability of explosion h50%) was measured as between 4-10 J by the Picatinny Arsenal apparatus and shown to be highly dependent on temperature, particle size and impurities.[71,73,74] (2) AgN_3 is generally accepted as being somewhat less sensitive than $Pb(N_3)_2$ (3) pure $Zn(N_3)_2$ remains poorly characterized, with indications that it explodes on minimal mechanical provocation[75] and mixtures of zinc with $Pb(N_3)_2$ are reported to form dangerously sensitive azide products.[76] Reports of zinc azide being insensitive are likely the result of its high hygroscopicity; hydrous (and most solvated) zinc azides are known to be insensitive,[77,78] with many reports of zinc azides offering poor description of the exact composition being tested.[74] (4) Impact sensitivity of LiN_3 has been measured to have an h50% of *ca* 22 J[74], although other sources quote it as completely insensitive.[19] For reference, it is worth noting that $Sn(N_3)_2$ is believed to have a similar sensitivity as its structural homologue, $Pb(N_3)_2$.[45] (*ca* 1.7 J by the Picatinny Arsenal apparatus[73]). (5) NaN_3 and NH_4N_3 are known to exhibit very low insensitivity.[79] However, debate remains, with recent work having suggested that impacts of *ca* 25 J can induce chemical decomposition in NaN_3 without a visible burn that is the typical characterization parameter of impact sensitivity testing.[80] (6) TAGZ has been found to have an h50% of *ca* 34 J.[81] (7) liquid and gaseous HN_3 are known to be highly sensitive,[74] although no sensitivity studies on crystalline[82] HN_3 are known.

A general experimental ordering can therefore be stated as NaN_3 ≈ TAGZ ≈ NH_4N_3 < LiN_3 < $Ba(N_3)_2$< AgN_3 < $Sn(N_3)_2$, with the exact positions of HN_3 and $Zn(N_3)_2$ remaining unknown.

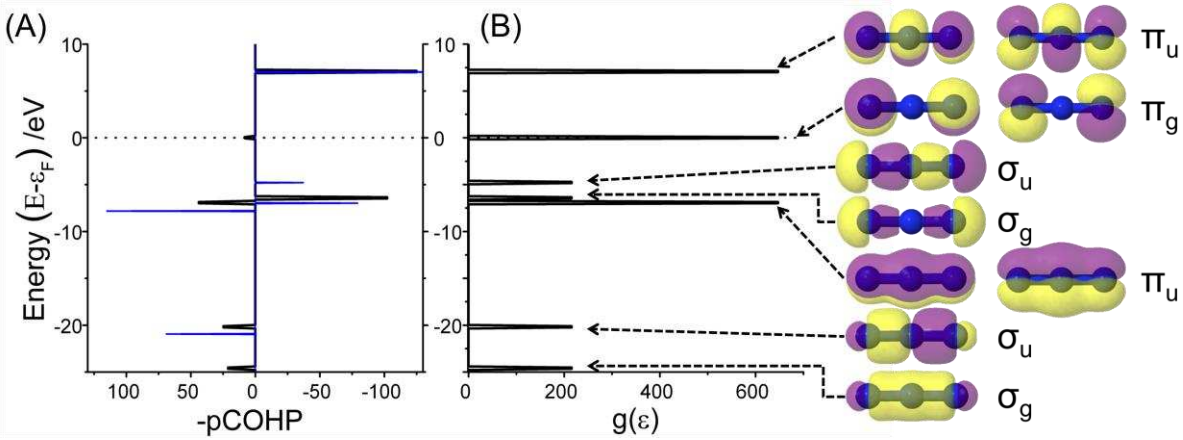

Fig 2: Electronic structure of the isolated N_3^- anion in a periodic box by HSE06. (A) The projected crystal overlap Hamilton population (pCOHP) is given for the identical N_1-N_2 and N_1-N_3 bonds. pCOHP is given for both a TZVP (black) and minimum STO-6G basis set (blue). (B) The orbital energies given as a density of states (g(ε)) calculated from a TZVP basis set. The corresponding canonical orbitals are given for each state.

Table 1: Test set of energetic azides used in this work, listed in approximate order of increasing sensitivity.

Material	Sensitivity Class*	Bond Type#	Ref.
NaN_3	I	I	[72]
TAGZ	LS	I	[81]
NH_4N_3	LS	I	[79]
LiN_3	LS	I	[74]
HN_3	S	M	[74]
$Ba(N_3)_2$	S	P	[71,72,74]
AgN_3	S	P	[83]
$Zn(N_3)_2$	S	P	[75]
$Sn(N_3)_2$	S	P	[45]

*Experimental sensitivity class according to indicated references. Sensitivity reported as insensitive (I), low sensitivity (LS), sensitive (S).

#Classification of bonding type: molecular (M), ionic (I) or polymeric (P)

Azide electronic structure: isolated molecule

A chemical explosion results from the rapid release of large quantities of potential energy stored within a molecule. For linear N_3^-, this is initiated through the rupture of a covalent N-N bond. In the ground equilibrium state, the N_3^- anion is closed shell ($^1\Sigma_u$) with R_{NN}= 1.1835 Å and θ_{NNN}=180°. The electronic structure of N_3^- is well characterized, with the highest occupied molecular orbital (HOMO) and lowest unoccupied molecular orbital (LUMO) adopting antibonding character, Figure 2. In order to study bond rupture, it is more instructive to analyze the nature of the HOMO and LUMO with respect to the individual covalent bonds: $R_1(N_1N_2)$ and $R_2(N_2N_3)$. This has been done by calculation of the projected Hamilton population (pCOHP), whereby the electronic density of states (DOS) is weighted by the Hamiltonian matrix element corresponding to the interaction between specific atoms. This technique has proven highly successful in the study of bonding structures within molecules and solids.[30,84–86]

As expected, the two σ states below -20 eV offer large bonding contributions (*i.e.* positive –pCOHP) to each of the N-N bonds, as does the π_u state at *ca.* -8 eV, Figure 2. The σ_g state at *ca* -7 eV instead shows a considerable antibonding character (*i.e.* negative –pCOHP) across directly bonded N atoms. The final occupied σ_u orbital at *ca* -4.5 eV is also expected to contain anti-bonding character, in line with analysis of the canonical orbital eigenvector. While it is effectively absent from the pCOHP calculation with a TZVP localized basis set (LBS), implying it is non-bonding, it shows notable antibonding character when derived from a minimum basis set (STO-6G). The π_g (HOMO) is expected to be non-bonding with respect to the individual N-N bonds, and therefore should be absent from the pCOHP. The presence of a small bonding structure in the pCOHP at this energy level suggests a small error associated with the projection of the Hamiltonian overlap elements onto the applied TZVP basis set. On moving to a minimum basis set, the expected absence of this interaction is obtained. Finally, the degenerate LUMO offers considerable antibonding character with respect to these individual N-N bonds with both basis sets.

In the ground state, extension of R_2 leads to bond dissociation at R_2 > 2 Å, with a dissociation energy of *ca* 4.5 eV, Figure 3A. The $|S_0,V_0\rangle$ $|S_1,V_0\rangle$ transition requires *ca* 5.1 eV energy. In this state, the energy barrier to bond dissociation is only *ca* 1 eV when $^{S_1}R_2$ > 1.75 Å, and once breached, dissociation is spontaneous, $\Delta E(^{S_1}R_{2,eqm} - {}^{S_1}R_{2,diss})$ ≈ -0.4 eV. Alternatively, transition to $|S_0,V_0\rangle$ $|T_1,V_0\rangle$ requires 4.21 eV excitation. In this state, the energetic barrier to bond dissociation is similar to the S_1 state (*ca* 1 eV when $^{T_1}R_2$ > 1.65 Å). As with the $^{T_1}R_2$ state, once this bond length is exceeded, bond dissociation is a favorable process [$\Delta E(^{T_1}R_{2,eqm} - {}^{T_1}R_{2,diss})$ ≈ -1.05 eV]. Note that the dissociation product of the T_1 state sits ≈ 1.2 eV below that

of the S_0 state. The same general trend is observed for all higher excited states. It therefore follows that excitation of the azido anion into any of the excited states favors bond dissociation, with considerable energy release. This agrees well with the LUMO orbital structure.

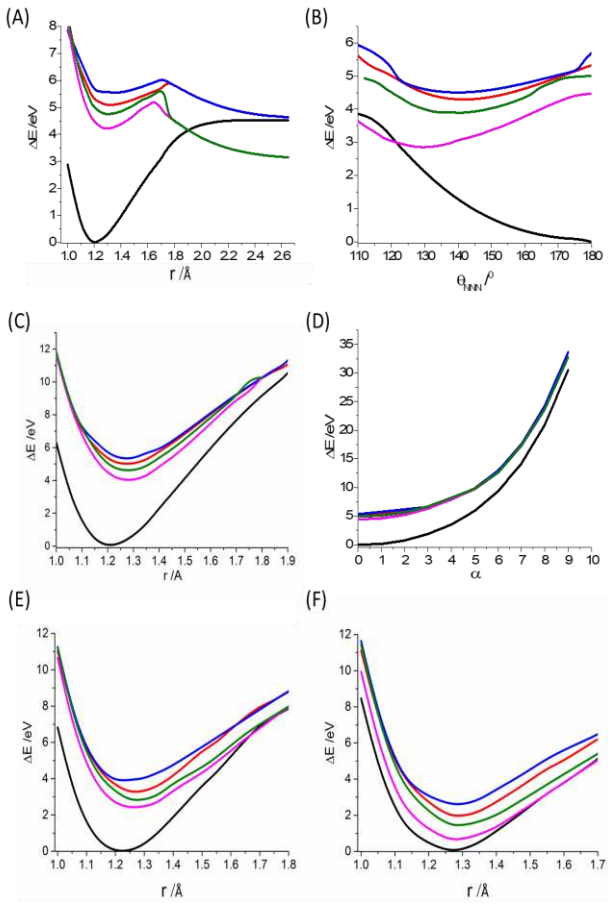

Fig 3: Potential energy surfaces (PES) associated with the N_3^- anion, based on MRCI calculations. PES are shown for (A) elongation of a single N...N covalent bond, and the three symmetry independent normal modes: (B) θ_{NNN}, (C) symmetric stretch, and (D) asymmetric stretch; $r_1=(r_{eqm} + \alpha/10)$, $r_2=(r_{eqm} - \alpha/10)$, where r_{eqm} is the equilibrium bond distance. The PES for the symmetric stretch at (E) θ_{NNN} = 150° and (F) θ_{NNN} = 130° are also given. In each case the potential energy surface for S_0 (black), S_1 (red), S_2 (blue), T_1 (pink) and T_2 (green) are given.

From a purely energetic perspective, the T_1 state appears to be the most likely candidate for bond dissociation. However, it is clear that the excitation energies required to reach any of the excited states far exceeds energies that are thermally available. Noting that impact induced detonation results from mechanical perturbation, it is prudent to instead consider a vibrationally induced process. The N_3^- molecule adopts the point group $D_{\infty h}$, with four normal coordinates: two degenerate orthogonal angle bends ($\delta\theta_{NNN}$; symmetry Π_u), an asymmetric stretch (δR_S; symmetry Σ_g) and a symmetric stretch (δR_A; symmetry Σ_u). The calculated frequencies for the isolated anion are found to be 668 cm^{-1}, 1355 cm^{-1} and 2127 cm^{-1}, respectively. This is consistent with experimental frequencies of 645 cm^{-1}, 1344 cm^{-1}, and 2041 cm^{-1},[46] noting that anharmonic effects, which are neglected here, are most important in the higher frequency modes. Variations in the electronic structure of the N_3^- molecule were then studied as a function of these normal modes, Figure 3B-D.

At the lowest frequency, $\delta\theta_{NNN}$ is most susceptible to mechanical perturbation. On deviation from 180°, the ground state increases in energy as θ_{NNN} decreases until an apparent plateau is achieved at *ca* 110°, with an overall increase in energy of *ca* 3.9 eV, Figure 3B. In contrast, the energy of the S_1 state decreases with θ_{NNN}, with a minimum energy separation between states achieved at *ca*. θ_{NNN} = 140° [$E(^{S1}\theta_{NNN}=180)$-$E(^{S1}\theta_{NNN}=140)$ = 1.1 eV], representing a reduction in the energy gap between the S_0 and S_1 state from over 5 eV to only 2.6 eV. The T_1 state also decreases in energy with angle bending to reach a minimum at *ca* θ_{NNN}=130° ($E(^{T1}\theta_{NNN}=180)$-$E(^{T1}\theta_{NNN}=140)$ = 1.7 eV), where the energy gap between the S_0 and T_1 states reduces from 4.2 to only 0.7 eV. Note this is less than the energy associated with the second overtone of the asymmetric stretching mode. On further bending, a conical intersection (CI) is observed between the S_0 and T_1 states at *ca*. θ_{NNN} = 120°. It therefore appears that across a small range of θ_{NNN}, the T_1 state remains energetically favored. Thus, the bending mode of the azido anion appears to offer a mechanism for the spontaneous electronic excitation of the molecule. It is also interesting to note that the change in the energy gap between the T_1 and S_0 state changes nearly linearly with increased angle bend at a rate *ca* 0.1 eV/°.

Discussion of the PES associated with the symmetric stretching mode (1355 cm^{-1}) of the N_3^- molecule is done with respect to the N-N bond length Figure 3C. This PES is notably different from the angle bend. As observed previously, the T_1 state exhibits the lowest energy amongst the excited states, with a $|S_0,V_0\rangle$ $|S_1,V_0\rangle$ transition of *ca*. 4 eV. In contrast to the bending mode, however, the extension of the eigenvectors of this mode are not associated with an obvious CI, even up to a bond stretch of 2.0 A, and carries an associated energy penalty of nearly 11 eV.

In order to assess the PES of the asymmetric stretch, we define the distortion parameter α, which represents the difference between the two bond lengths R_1 and R_2. In this way, the PES for the asymmetric stretching mode (2127 cm^{-1}) is followed, Figure 3D. Due to contraction of R_2, the energy is found to rise considerably faster than for the symmetric mode. We note, however, that no CI is observed below an energy penalty of 30 eV as a result of this normal mode.

Finally, it is interesting to consider a combination of the two most labile modes, the angle bend and symmetric stretching modes. At an angle bend of 150°, the PES of the symmetric stretching mode changes slightly from that observed for the linear molecule, Figure 3E. Most notably,

the CI can now be achieved by extension of the bond stretch to *ca.* 1.65 Å. On bending further, to 130°, the S_0/T_1 CI occurs at just 1.4 A, Figure 3F. Thus it would appear that a thermally accessible reduction in the frontier orbitals of the azido anion can be accessed upon stretching the N–N bond, provided the anion is bent.

Given that the proposed non-adiabatic intersystem crossing between the S_0 and T_1 states at the CI requires a change in spin, spin-orbit (SO) coupling should be taken into account in the simulation. At the identified CI, the SO coupling associated with S_0/T_1 transition (based on the S_0 geometry) was found to be *ca* 10 cm^{-1}, *i.e.* a small effect. This is in line with typical values for organic molecules.[87]

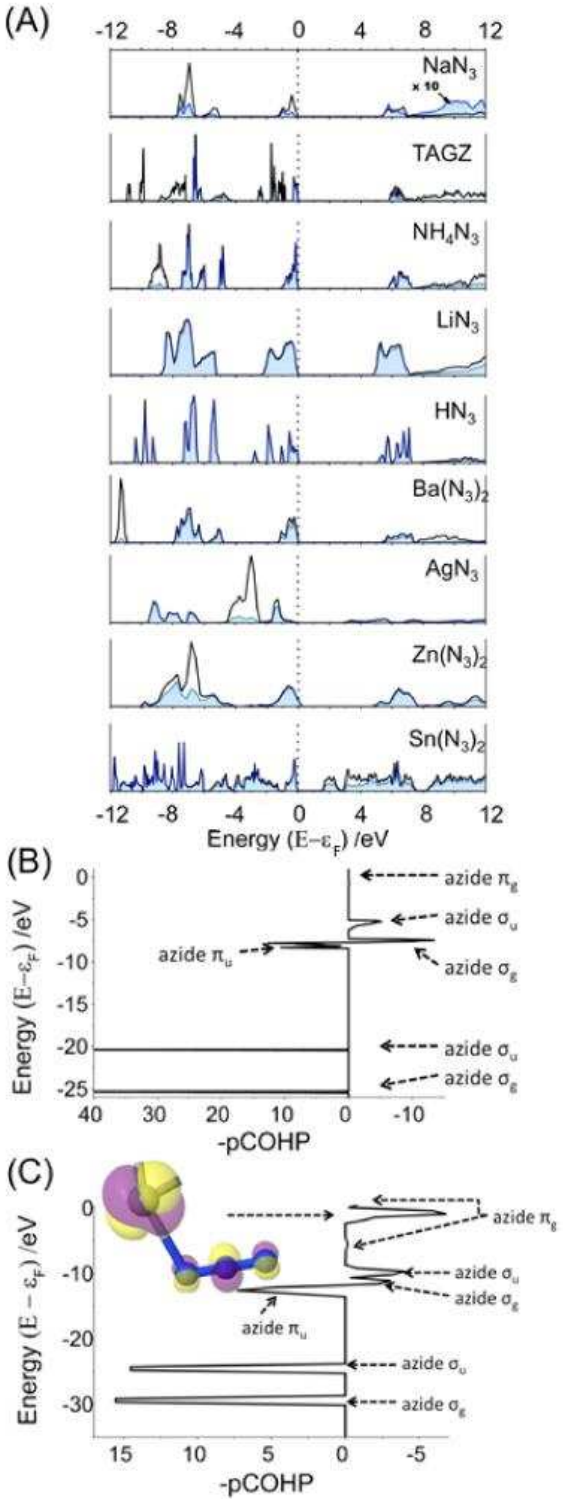

Fig 4: Electronic structure of the crystalline azide materials. (A) The total DOS (black) and azide channel (blue). pCOHP analysis given across the equivalent N-N azide bonds for (B) NaN_3, and (C) AgN_3 (Others in ESI). Orbitals are labeled according to symmetry of Figure 2. ε_F = 0 in all cases.

Azide Electronic Structure: Crystalline Lattice

While discussion of the isolated gas-phase azide anion offers insight into a pathway to detonation, it cannot

explain the breadth of impact sensitivities of the anion within different crystal lattices. It is therefore necessary to understand the effect of the counter ion and the crystal environment on the electronic structure of N_3^-. This can again be achieved by analysis of the associated electronic DOS and pCOHP.

To the best of our knowledge, no experimental band structures exist for the inorganic azides. Thus, as a benchmark, a 'band gap' was generated for the isolated azido anion using the HSE06 screened hybrid DFT functional[67] and a localized Gaussian basis set, Table 2. This functional introduces exact Hartree-Fock exchange, reducing the well-known self-repulsion error associated with GGA-derived band gaps.[88] Band gaps calculated with this function have been shown to agree closely with experiment.[68] For isolated N_3^- the HSE06 HOMO-LUMO gap is found to be 7.06 eV, Figure 2 (compared to 5.64 eV by PBE). We note that this value is somewhat larger than the $|S_0,V_0\rangle$ $|S_1,V_0\rangle$ transition in Figure 3(a), with a vertical excitation energy of *ca* 5.5 eV. This stems in part from the applied basis set, and must include variability due to the theory applied (DFT vs MRCI). It is also worth noting that the excited state orbitals in the MRCI method do not take the canonical forms as calculated for ground state structures by DFT. The electronic 'density of states' (DOS) and associated pCOHP for the isolated N_3^- ion according to HSE06 calculations were given in Figure 2.

The electronic band structure was calculated for each of the crystalline azide materials in the test set using the PBE GGA (with plane waves, PW, and localized basis set, LBS) and HSE06 (with LBS) hybrid DFT functionals. It is generally seen that the band gap agrees well between PW and LBS PBE calculations, Table 2, and suggests that the choice of basis set is adequate in the latter.[89] The trend in PBE band gaps fits well with earlier reports that the larger the band gap, the less sensitive the material.[90] However, we do note some discrepancies in ordering, particularly for NaN_3 and $Ba(N_3)_2$. As expected, the value of the band gap for each azide increases on moving to the hybrid HSE06 functional, Table 2. Interestingly, while the sensitivity / band gap trend holds relatively well for the GGA functional PBE, it is less prominent for the higher-level functional HSE06. As the latter is expected to be notably more accurate, this suggests that the correlation with the lower level functional was largely fortuitous. Some earlier works also show discrepancy between sensitivity and band gap.[91]

Noting that chemical detonation must primarily involve the electronic structure of the azido anion, it is useful to decompose the band structure into its atomic contributions. The azido anion N-channel band structure closely reproduces that of the isolated anion in each case (compare Figure 4(b,c) with Figure 2(a)). Some broadening is observed and reflects a degree of mixing within the solid state. This holds true for many of the azides, with the notable exceptions being the Ag and Sn based materials, as well as for the molecular azide, HN_3. Analysis of the pCOHP across the series of azides (ESI) shows that the character of the majority of electronic states of the azido anion remain unchanged up to the HOMO-1 σ_u orbitals, while covalent interactions of the azido anion with the cation leads to a splitting of the higher-lying π_g state into two features (near ε_F and *ca* -4 eV; STO-6G basis set energies). There is notable anti-bonding character observed near the Fermi level, ε_F. Analysis of the canonical crystal orbitals (ESI S4) suggests that the original molecular π_g orbitals remain non-bonding at ε_F. However, new orbitals appear at ε_F, which contain anti-bonding π_u character. This causes broadening of the N-channel DOS, Figure 4(a), in both valence and conduction bands. Importantly this interaction also leads to an overall increase in the antibonding character of the high-lying occupied states, with respect to individual N–N bonds. This is most notable for the covalent azides, and suggests that the equilibrium structure of these materials may already display weakened N–N bonds, more easily broken on mechanical perturbation. Overall, the stronger the covalent interaction with the N_3^- HOMO orbitals, the smaller the electronic band gap and the greater the anti-bonding character observed across the valence bands, ESI.

Despite minor differences in the N-channel electronic structure, the general nature of the orbitals around ε_F remain the same in all of the crystalline materials studied here, as confirmed by analysis of the canonical orbitals and pCOHP analysis (ESI S4). Furthermore, ε_F and the lowest conduction band always contain notable N_3^- character. As a first approximation, it can therefore be assumed that the general trends observed for the electronic excitation processes will hold across the materials. We note that the PES in Figure 3 correspond to electronic excitation of the azido anion, rather than a reduction of the molecule. Thus it is worthwhile considering only the N-channel band gap, eliminating effects of the metal to azide electron transfer. This has little effect on the electronic band gaps.

It is interesting to note that in all cases, the band gap (which corresponds to the HOMO-LUMO canonical orbitals in the ionic azides) is considerably less than for the isolated azido anion, Table 2. Noting that for the ionic materials there is negligible counter ion character in the top valence and bottom conduction band, this cannot result from mixing. Instead, we suggest this to occur as a result of Coulombic (dielectric) screening[92,93] of the azido anion 'band gap' by the counter ion. The reduction in band gap is least for the 'softest' counter ion (TAGZ), with band gap decreasing as a function of ionic 'hardness' : TAGZ > NH_4N_3 > NaN_3 > LiN_3. This is most notable for the isostructural NaN_3 and LiN_3 salts, whose band gaps correspond well with previous calculations.[89] This may offer a design tool for production of novel energetic materials.

Table 2: Calculated band gaps (in eV) for the azides. PBE band gaps were calculated by both PW and LBS methods, and the HSE06 band gaps by LBS methods.

Material	PBE (PW)	PBE (LBS)	HSE06	D/ID
N_3^-	--	5.64	7.06	--
NaN_3	4.00	4.02	5.27	D
TAGZ	4.47	4.48	5.82	ID
NH_4N_3	4.07	4.36	5.65	ID
LiN_3	3.75	3.56	4.75	D
HN_3	3.813	3.78	5.20	ID
$Ba(N_3)_2$	-	4.12	5.32	D
AgN_3	1.81	1.57	2.77	D
$Zn(N_3)_2$	-	3.41	4.78	ID
$Sn(N_3)_2$	0	0.66	1.51	ID

D/ID indicate direct or indirect band gap. Suitable Zn and Ba basis sets were not available for PW-PBE calculations

Structure and Sensitivity

From the previous discussion it is clear that athermal electronic excitation of the crystalline azide materials must be the result of a non-adiabatic, vibronic process. This process appears to be primarily controlled by access to the N_3^- bending mode. However, the magnitude of the bending motion that is required to reach a CI is well beyond that achievable under equilibrium conditions. It follows that a critical process in the initiation mechanism rests in obtaining a vibrationally excited state of the N_3^- bending motion. This can be achieved by phonon *up-conversion*, which results from phonon-phonon collisions.

Vibrational Structure

The ability of vibrational energy to up-convert depends on the underlying vibrational structure. To this end, phonon dispersion curves were calculated within the harmonic approximation for each of the systems studied here, and the corresponding phonon density of states (PDOS) generated, Figure 5 and ESI S3. In all of the present materials, there are two very distinct clusters of frequencies in vibrational space: the low-lying external modes, and the higher frequency internal modes. Based on established processes of tribomechanics, the energy of a mechanical impact is injected into the zone-centre (Γ-point) acoustic modes as a compressive wave (or other low frequency external modes if non-covalent bond rupture processes are considered).

The following discussion is restricted to within the third anharmonic approximation for phonon scattering. Within this approximation, the rate of energy transfer, $\gamma_{j,\boldsymbol{q}}$, into a vibrational mode with branch index *j* and wave vector **q** is defined by Equation 2.[94] The square brackets contain two terms and describe two energy conversion processes, respectively. The first is the down conversion of energy, as a frequency $\omega_{\boldsymbol{q}j}$ decays into two low-frequency phonons, $\omega_{\boldsymbol{q}'j'}$ and $\omega_{\boldsymbol{q}''j''}$. The second is the combination of two phonons $\omega_{\boldsymbol{q}j}$ and $\omega_{\boldsymbol{q}'j'}$ to form a third, $\omega_{\boldsymbol{q}''j''}$. When $\omega_{\boldsymbol{q}''j''} > \omega_{\boldsymbol{q}j}$, this process is known as *up-pumping*. Conservation of energy is maintained by use of the Dirac δ, and momentum is conserved by setting $\boldsymbol{q} = -\boldsymbol{q}'-\boldsymbol{q}''$. The number of scattering processes is temperature dependent through the Bose-Einstein statistical occupations of the coupling phonon modes ($n_{\boldsymbol{q}'j'}$). The efficiency with which each combination of phonons scatter is dependent on an anharmonic coupling constant, $V^{(3)}$, which itself depends on the relative polarization and anharmonic character of the three coupling phonon modes. To achieve a highly excited state of a target vibrational mode, it is important to achieve rapid conversion *into* the corresponding branch. The slower the conversion into the branch, the more the required input energy to achieve sufficient excitation.

$$\gamma_{\boldsymbol{q},j} = \frac{\pi}{\hbar^2 N_q}\sum_{\boldsymbol{q}',j',j''}\left|V^{(3)}_{\boldsymbol{q}j,\boldsymbol{q}'j',\boldsymbol{q}''j''}\right|^2 \times \left[\left(1+n_{\boldsymbol{q}'j'}+n_{\boldsymbol{q}''j''}\right)\delta\left(\omega_{\boldsymbol{q}j}-\omega_{\boldsymbol{q}'j'}-\omega_{\boldsymbol{q}''j''}\right)+2\left(n_{\boldsymbol{q}'j'}-n_{\boldsymbol{q}''j''}\right)\delta\left(\omega_{\boldsymbol{q}j}+\omega_{\boldsymbol{q}'j'}-\omega_{\boldsymbol{q}''j''}\right)\right] \quad \text{Equation 2}$$

It follows from Equation 2 that energy transfer rates will be faster when including low frequency modes (higher population) or highly anharmonic modes. Mechanical impact can be treated as instantaneous heating of the lowest frequency vibrational modes, from which it follows that the population of the lowest frequency modes will be very high, permitting rapid up-conversion. In the present contribution the explicit effects of temperature will be neglected; the extension of the current model to variable temperature processes will be the subject of follow-up work. For simplicity, we note that the upward drive of energy due to high population of low frequency modes is the starting point for the model presented here.

In the absence of temperature effects, it is convenient to employ a base model, structured at the low temperature limit. At 0 K, Equation 2 reduces to,

$$\gamma_{\boldsymbol{q},j} = \frac{\pi}{\hbar^2 N_q} \sum_{\boldsymbol{q}',j',j''} \left| V^{(3)}_{\boldsymbol{q}j,\boldsymbol{q}'j',\boldsymbol{q}''j''} \right|^2 \times \left[\delta\left(\omega_{\boldsymbol{q}j} - \omega_{\boldsymbol{q}'j'} - \omega_{\boldsymbol{q}''j''} \right) \right]$$

Equation 3

Here the bracketed term represents the two-phonon density of states, $\Omega^{(2)}$, and offers a count for the number of coupling pathways that link a high frequency mode $\omega_{\boldsymbol{q}j}$ to two lower frequency modes. In the absence of population in this low temperature limit, microscopic reversibility dictates that the number of down-conversion pathways must be equivalent to the number of up-conversion pathways. Hence, in the limit of T=0K, Equation 3 describes the energy transfer rates. In this form, we define $\omega_{\boldsymbol{q}j}$ as the target frequency (now labelled $\omega_{\boldsymbol{T}}$, the N_3^- bending mode), with $\omega_{\boldsymbol{q}'j'}$ and $\omega_{\boldsymbol{q}''j''}$ denoting lower frequency modes. Energy transfer to $\omega_{\boldsymbol{T}}$ is therefore largely dependent on the number of pathways defined by $\Omega^{(2)}$.

Before deeper consideration of Equation 3, it is convenient to introduce a clustering of the PDOS, which follows from the three terms contained within $\Omega^{(2)}$.[56] The first mode, $\omega_{q'j'}$ generally exhibits lattice character, and is held within the phonon bath, which has an upper limit of Ω_{max}. While this value is not rigorously defined, it can be qualitatively described as the highest lattice-based mode. It is generally identified by a notable gap in the PDOS. The second frequency, $\omega_{q''j''}$, generally sits somewhere between Ω_{max} and $2\Omega_{max}$, and is termed the 'doorway mode'. The upper limit of $2\Omega_{max}$ is significant as it defines the highest frequency attainable by coupling of two phonon bath modes.

Careful study of the zone-centre eigenvectors allowed identification of $\omega_{\boldsymbol{T}}$ (ESI S5). This is taken to be the mode characterized by θ_{NNN} behavior, Figure 5. For the more highly covalent compounds, multiple modes with θ_{NNN} character exist, owing to the symmetry breaking of the N_3^- molecules. With the exception of HN_3, all materials exhibit the expected bending mode at *ca* 600 cm^{-1}. For the cases of $Sn(N_3)_2$ and $Zn(N_3)_2$ there are two distinct clusters of modes that exhibit θ_{NNN} behavior. These correspond to a coupling between θ_{NNN} and θ_{MN}, where M is the corresponding metal cation. Importantly, the existence of this second mode gives rise to a lower frequency normal coordinate with considerable θ_{NNN} character. The presence of this mode seems to correlate with the presence of strong covalent interactions between the azido anion and cation species and may offer insight into a potential target for the design of new energetic materials.

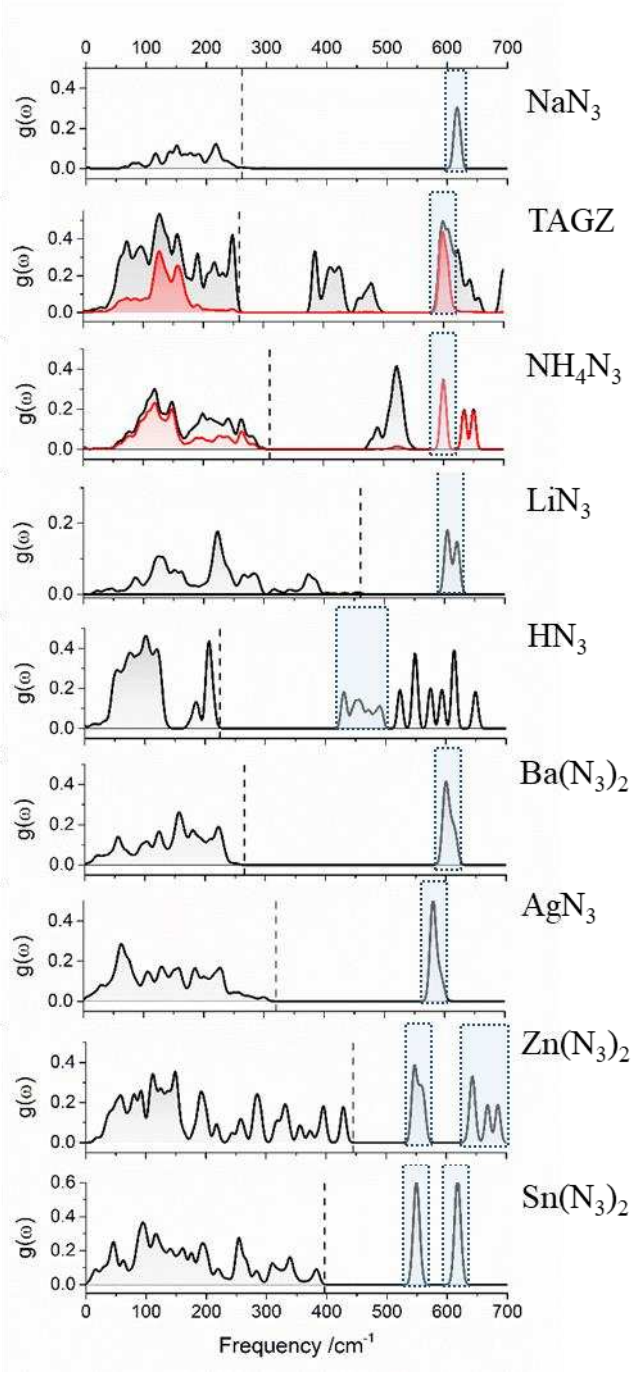

Fig 5: Phonon density of states for the crystalline azide materials studied here. The target frequencies are indicated in blue and Ω_{max} with a vertical dotted line. For the molecular cationic materials, the N_3^-partial DOS is given in red.

The position of Ω_{max} is important, as the anharmonicity of $\omega_j < \Omega_{max}$ leads to a rapid population equilibration of these modes in accordance with both up- and down-conversion processes of Equations 2 and 3. Experimental work has suggested that this equilibration occurs at least an order of magnitude faster than any up-conversion beyond Ω_{max}.[40] Thus, at finite temperature (where $\omega_j >$

Ω_{max} have a population > 1) the transfer of excess energy resulting from a mechanical perturbation must include *at least* one mode with $\omega_j < \Omega_{max}$. As temperature decreases, the probability of up-conversion processes therefore diminish, as do energetic sensitivities.[83] The probability of phonon-phonon coupling processes is governed by Fermi's Golden rule,[95]

$$\wp(i \to f) \propto \left|\langle \varphi_f | H_3 | \varphi_i \rangle\right|^2 D_f(E) \qquad \text{Equation 4}$$

where $D_f(E)$ is the density of final states and H_3 is the third order anharmonic Hamiltonian. Thus, the probability ($\wp$) of scattering is a maximum when the initial and final scattering states, $|\varphi_i\rangle$ and $|\varphi_f\rangle$, respectively, are coherent. Qualitatively, it follows that the greater the total change in the PDOS, the less probable the transition will be. Within the nomenclature introduced above, we might therefore expect that energy transfer to ω_T will occur more quickly given a smaller $\Delta\omega = \omega_T - \Omega_{max}$. We note that the presence of doorway modes generally further increases the probability of scattering. Analysis of this value for the compounds studied here does suggest some merit to this qualitative methodology, Table 3, although discrepancies do arise. This is most notable with LiN_3 and $Ba(N_3)_2$, which appear in notably different classifications according to this method. Thus, a simple correlation based on the interpretation of Equation 4 (i.e. solely on Δω), while potentially indicative in the first instance, is insufficient to provide relative ordering of sensitivity.

Table 3: Characteristic vibrational frequencies for the crystalline azide materials, Zone-centre target frequency ($\omega_T(\Gamma)$) and phonon bath maximum, Ω_{max}, are given, alongside the associated frequency gap.

Material	$\omega_T(\Gamma)$ /cm^{-1}	Ω_{max} /cm^{-1}	$\Delta\omega$ /cm^{-1}
NaN_3	615	250	365
TAGZ	595	260	335
NH_4N_3	605	310	295
LiN_3	605, 620	460	145, 160
HN_3	435-500	225	210-275
BaN_3	600, 615	265	335, 350
AgN_3	581, 594	320	261, 274
ZnN_3	547, 630, 670, 685	445	102, 185, 225, 240
SnN_3	550, 615	395	155, 220

As is generally the case with the vibrational structure of molecular materials, the branches (i.e. wave vectors, **q**) corresponding to internal modes are relatively flat. Following from this, we can make an approximation to simplify the coupling pathways available for up-conversion. Within the first anharmonic approximation of phonon-phonon interactions, coupling is restricted to three phonons, where momentum and energy are strictly conserved. A flat ω_T (i.e. $\boldsymbol{q}$ invariant) means that the scattering of two low-frequency modes of any momentum can be considered, provided they meet the energy requirements. Thus, the Dirac δ of Equations 2 and 3 can be simplified to $\delta(\omega_j - \omega_{j'} - \omega_{j''})$. We note that while it is in principle possible to explicitly calculate the value of $V^{(3)}$ for each scattering process (and has been done by way of example for a single system in this case, ESI S6),[94] the magnitude of the calculation is infeasibly large for the current systems of interest, and has therefore not been pursued in the following discussion. This approximation further allows us to consider vibrational coupling by means of the PDOS, rather than from the ($\boldsymbol{q}$ variant) complete dispersion curves.

We again note that within the first anharmonic approximation, only two phonons ($\omega_{j'}$ and $\omega_{j''}$) may scatter to form a third (ω_T). For instance, $\omega_{j'}$ and $\omega_{j''}$ which share the same branch index and frequency, i.e. $\omega_{j'} = \omega_{j''}$ could scatter, but this imposes the restriction that $\mathbf{q}(\omega_{j'})$ = - $\mathbf{q}(\omega_{j''})$, and $\mathbf{q}(\omega_j)$ = Γ. For ease of discussion, we shall adopt the spectroscopic term *overtone* to refer to this scattering mechanism. Alternatively, if $\omega_{j'} \neq \omega_{j''}$ modes scatter such that $\mathbf{q}(\omega_j) = \mathbf{q}(\omega_{j'}) + \mathbf{q}(\omega_{j''})$ then this conforms to the spectroscopic term *combination.* Explicit calculation of these coupling pathways suggests that for the ionic azides, only the phonon modes that contain N_3^- character couple efficiently to internal N_3^- vibrational modes (ESI S6). Thus, for the remainder of this discussion, only the N-channel PDOS will be considered for the ionic azide materials. This appears to be an important consideration for the design of novel materials. The full set of PDOS are shown in Figure 5.

In accordance with Equation 4, overtone pathways can be expected to occur more efficiently. This assumption formed the base for previous work at understanding impact sensitivity.[37,39] However, the number of overtone pathways is far fewer than the pathways available by the

combination mechanism. Further, only the first overtone pathway can be considered within the first anharmonic approximation. Higher order overtones become increasingly improbable, making these pathways less likely for materials in which $\omega_T > 2\Omega_{max}$. In the case of the azides, this affects NaN_3, TAGZ, and BaN_3.

To account for overtone pathways the PDOS $g(\omega)$ is simply scaled by N, the overtone number,

$$g^N(\omega) = \frac{g(\omega)}{N}\,;\, \omega^N = \omega N \qquad \text{Equation 5}$$

The number of pathways available for energy transfer (*i.e.* the rate of vibrational up-conversion) within this model can then be taken as an integration of $g^N(\omega)$ at each $\boldsymbol{\omega_T}$. To account for slight errors in the calculated vibrational frequencies (due to *e.g.* anharmonicity and limitations of computational theory), and the existence of resonant vibrational states, a sampling window of $\omega_T \pm 10$ cm^{-1} was used, reflecting the Gaussian smearing applied in generation of the DOS, Figure 6. Changes to this target window do not affect the relative predicted sensitivity ordering (ESI S7).

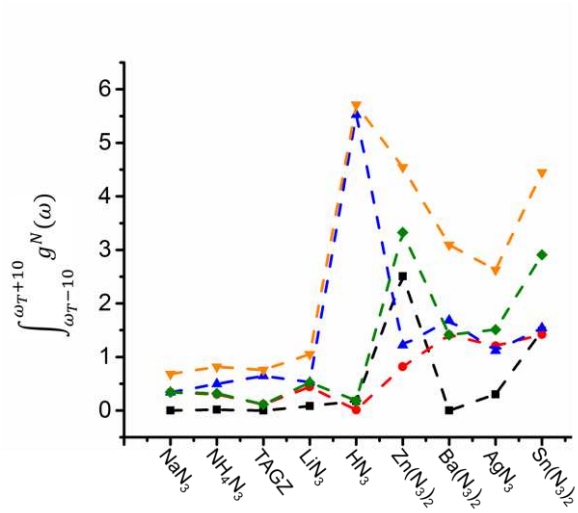

Fig 6: Integration at $\omega_T \pm 10$ cm^{-1} for the overtone pathways available in the crystalline azide materials, arranged in approximate order of increasing sensitivity. Values are given as sums across all target modes. Overtones N=2 (black), N=3 (red) and N=4 (blue) are shown, alongside N2+N3 (green), as well as N2+N3+N4 (orange).

As a general trend, it is found that the sum of $g^N(\omega_T)$ is greater for the more sensitive materials (i.e. towards the right in Figure 6). However, the correlation is insufficient for the overtone pathway model to properly account for the varying sensitivities of the energetic azides. This deficiency is particularly notable for the low sensitivity materials and HN_3, which is indistinguishable from the insensitive materials. In order to consider combination pathways, we generate $\Omega^{(2)}$ for each of the materials under investigation, Figure 7. This is done by only considering the pathways in which both $\omega_{q'j'}$ and $\omega_{q''j''} < \omega_T$, thus ensuring only up-conversion processes are considered. To further adhere to the model proposed in the *General Theory* section, further constraints are imposed on generation of $\Omega^{(2)}$, ensuring that $\omega_{q'j'}$ and $\omega_{q''j''} < 2\Omega_{max}$ and $\omega_{q'j'} < \Omega_{max}$. This forces all values of $\Omega^{(2)} < 3\ \Omega_{max}$ to include at least one phonon mode, and ensures that modes neighboring ω_T do not inappropriately act as doorway modes if $> 2\Omega_{max}$. Generally this restriction has little effect on the structure of $\Omega^{(2)}(\omega_T)$, Figure 7. As a general trend it is seen that ω_T sits within the restricted $\Omega^{(2)}$ for sensitive materials, with little to no $\Omega^{(2)}$ density found at ω_T for insensitive materials. The magnitude of $\Omega^{(2)}$ is seen to increase notably with increasing sensitivity (i.e. from top to bottom of Figure 7). Only one exception ($Ba(N_3)_2$) is found to this trend. Despite its similarity to the PDOS of AgN_3, the lower value of Ω_{max} for $Ba(N_3)_2$ means that ω_T sits just beyond the doorway region. Thus, the magnitude of $\Omega^{(2)}$ is necessarily zero, given no doorway modes are present. The calculated Γ-point Ω_{max} of $Ba(N_3)_2$ agrees well with experimental measurements (230-240 cm^{-1})[96] and suggests minimal error in our selection of the phonon bath for this material.

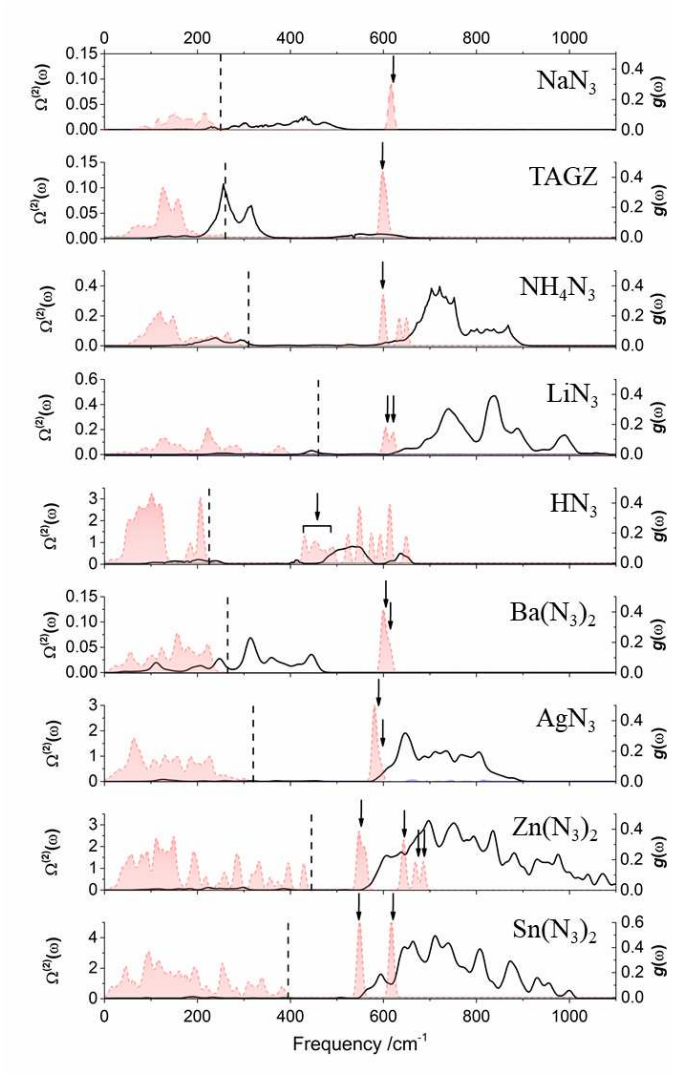

Fig 7: Two phonon density of states (2PDOS; $\Omega^{(2)}$) for the azides, calculated by enforcing both $\omega_{\boldsymbol{q}'j'}$ and $\omega_{\boldsymbol{q}''j''}$ < $2\Omega_{max}$ (black). The PDOS is given in red. Ω_{max} is given as a vertical dotted line, and $\omega_{\boldsymbol{T}}$ is indicated with an arrow.

By imposing the approximation that the target band is flat in each case, the value of $\Omega^{(2)}$ at the target frequency is indicative of the number of coupling pathways available to transfer energy to a particular $\omega_{\boldsymbol{T}}$..Based on this simple approximation, a good correlation is already found between the value of $\Omega^{(2)}(\omega_T)$ and the experimental impact sensitivity for each compound, Figure 8 and ESI S8. The insensitive materials are found to have $\Omega^{(2)}(\omega_T) \approx 0$, and indicates that in the ideal crystal, they cannot be easily initiated by impact. This is consistent with experimental reports for these materials. As the experimental sensitivity increases, so does the value of $\Omega^{(2)}(\omega_T)$. However, by enforcing $\omega_{\boldsymbol{q}'j'}$ and $\omega_{\boldsymbol{q}''j''} < 2\Omega_{max}$ and $\omega_{\boldsymbol{q}'j'} < \Omega_{max}$, $Ba(N_3)_2$ is also predicted to be an insensitive material, Figure 8(a). It is worth noting that the slope of $\Omega^{(2)}$ for $Ba(N_3)_2$ is very steep, and a small change in target frequency, or integration window, introduces a considerable shift in its predicted sensitivity. The same is not true of the other materials. From an experimental perspective, this suggests that the introduction of defects, or the compression associated with a shock wave, may act to drastically increase the sensitivity above the 0 K predicted levels reported here. Such effects have been reported.[71]

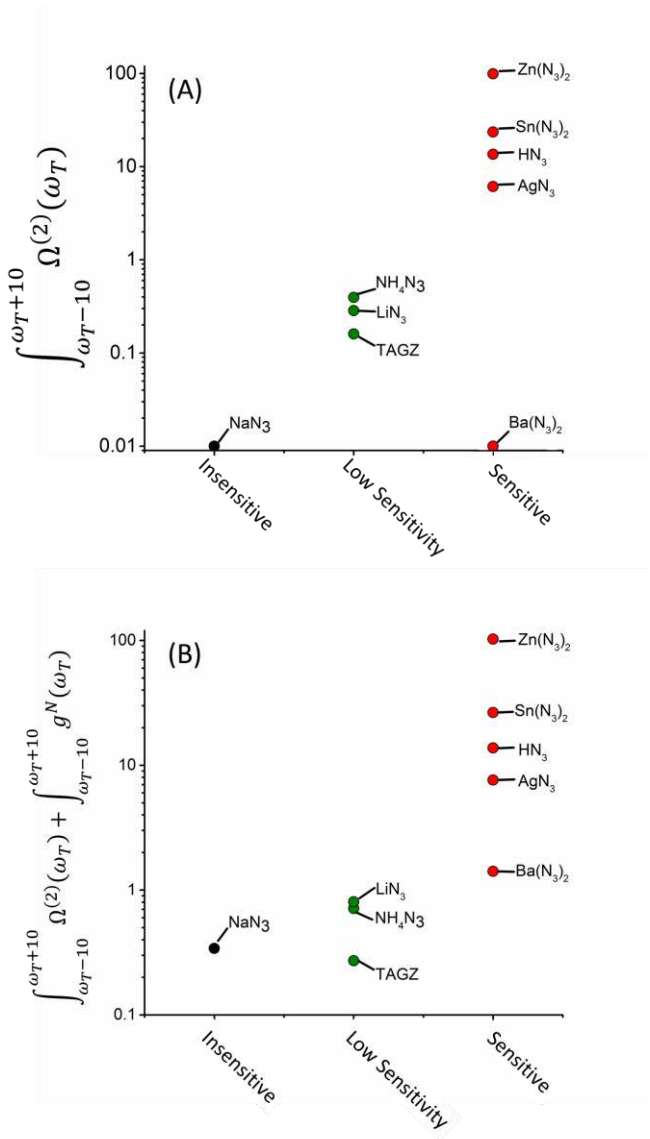

Fig 8: Integrated $\Omega^{(2)}(\omega_T)$ for the azides. (A) Based on $\Omega^{(2)}$ generated under the restriction of $\omega_{\boldsymbol{q}'j'}$ and $\omega_{\boldsymbol{q}''j''} < 2\Omega_{max}$ and $\omega_{\boldsymbol{q}'j'} < \Omega_{max}$. (B) Recasting of (A) with addition of $g^N(\omega_T)$ for N=2,3.

As a final step the possible energy coupling pathways available through overtones must now be considered. Given the high anharmonicity of phonon modes, experiments have suggested quartic coupling remains feasible (*i.e.* N=3). If these pathways are finally

considered, the predicted ordering becomes very promising, Figure 8(b). $Ba(N_3)_2$ is now predicted to be somewhat less sensitive than AgN_3, and LiN_3 is found to bridge between the low and high sensitivity compounds.

The exact ordering of energetic sensitivities is widely debated in the literature. For example, the relative ordering of $Ba(N_3)_2$ and AgN_3 is debated, with most recent reports suggesting AgN_3 > $Ba(N_3)_2$.[19] The sensitivity of $Zn(N_3)_2$ has also been debated, with some reports suggesting its sensitivity to be greater than that of $Pb(N_3)_2$, acting as a sensitizer.[76] Many of these discrepancies are likely due to experimental conditions (particle size, crystallinity, impurities, etc). In the present contribution, the sensitivity of the *ideal* crystalline material is considered. The model outlined in the *General Theory* section yields a highly promising method to determine the relative sensitivity ordering of energetic materials. We believe it is also useful to assist in the classification and ordering of energetic materials where highly debated experimental reports exist. Based on this work, we therefore propose a sensitivity ordering of NaN_3 ≈ TAGZ < NH_4N_3 < LiN_3 < $Ba(N_3)_2$ < AgN_3 < HN_3 < $Sn(N_3)_2$ < $Zn(N_3)_2$. This appears to be consistent with experimental reports.

At present many questions remain surrounding the exact relation between impact sensitivity and the $\Omega^{(2)}(\omega_T)$ values presented here. We also note that a true correlation must also consider any differences associated with the subsequent electronic excitation processes. However, despite the simplifications presented here, it is highly encouraging to find that for systems that are initiated by the same normal mode of the same energetic molecule, this complex process can be largely reduced to consideration of $\Omega^{(2)}(\omega_T)$.

CONCLUSION

Azides represent a broad class of energetic compounds ranging in impact sensitivity from completely insensitive to extremely sensitive. Noting that chemical detonation requires breaking of a chemical bond (*i.e.* an electronic process), the electronic structure of the N_3^- molecule was investigated. Athermal bond rupture was found to be possible through excitation of the N_3^- bending mode *via* a vibronic coupling process to the T_1 electronic state. The electronic structure of the N_3^- anion was found to vary little across the crystalline materials investigated. This indicates that the same electronic excitation process should be present in all of these materials. It was found that consideration of the rate of energy up-conversion into this target N_3^- bending mode is sufficient to gain a reliable sensitivity ordering of the azide series of compounds. Thus, we demonstrate here the first fully *ab initio* approach to the prediction of the relative impact sensitivities of energetic azides, and identify a means to lift the empirical assumptions on Ω_{max} imposed in previous, related models for other systems. The rate of up-conversion is found to be largely dependent on two key vibrational frequencies: 1) the maximum phonon frequency, Ω_{max}, and 2) the frequency of the N_3^- bending mode, ω_T. Determined by the external lattice modes, the former is largely dependent on the crystal packing structure. Modifications (polymorphism, co-crystallisation, crystal doping, pressure, temperature, etc.) can therefore all be expected to be useful tools to modify this parameter. Stronger bonding of the N_3^- anion within the lattice (*i.e.* those composed of polymeric or strongly hydrogen bonded structures) generally lead to a higher Ω_{max}. It also follows that more compressible materials will exhibit a higher Ω_{max} when subject to a mechanical perturbation. The second frequency, ω_T, depends on the bonding nature of the N_3^- anion within the crystal lattice. Higher covalency has been found to decrease ω_T, and thus enhance sensitivity. The increased covalent character between the N_3^- molecule and a cation also appears to weaken the N-N bond, rendering initiation easier. This again offers a design route to developing novel materials with targeted properties.

The present model encompasses, in part, many of the preceding models that have been used to describe impact sensitivity. For example, there is a clear rationale for the correlation of band gap, bond dissociation energy, etc, with impact sensitivity. Further, effects such as packing density and crystal packing can all find a physical basis within this model. We therefore suggest that previous attempts at correlating individual structural or electronic features with impact sensitivity may be in part correct, albeit without the full interpretation. We also note that within this theory, the known increase in sensitivity with pressure can also be explained through enhanced vibrational anharmonicity on compression. All models for impact sensitivity can find some root within the theory presented here.

While the present model has successfully predicted the relative ordering of the ideal crystalline structures of the energetic materials tested here, it is not yet capable of describing the exact energies required to initiate detonation. A complete, fine-tuned model will require consideration of the exact energy conversion rates and

electronic excitation processes. The current model is not yet capable of modelling composite or defective energetic materials. Thus, the trends predicted here reflect the intrinsic sensitivity of the ideal crystalline state. It is also worth noting that, while this model offers a powerful means to classify the relative sensitivity ordering of energetic materials, it is not yet capable of determining *if* a material should be expected to be energetic at all. These areas continue to offer immense scope for future development. However, the present contribution offers a powerful platform from which novel materials can be designed *in silico*, and offers novel insight into the structure-property relationships of common energetic materials.

AUTHOR INFORMATION

Corresponding Author

*carole.morrison@ed.ac.uk.

Author Contributions

The manuscript was written through contributions of all authors. All authors have given approval to the final version of the manuscript.

ACKNOWLEDGMENT

The authors thank an Edinburgh Global Research Scholarship (AM), EPSRC CMAC EP/Io33459/1 (AM) and DSTL (CAM) for funding. Thanks to the UK Materials and Molecular Modelling Hub for computational resources, partially funded by EPSRC (EP/Po20194/1). Additional thanks to the Edinburgh Compute and Data Facilities (ECDF) for further computational resources. Final thanks to Prof A. Cumming, Dr A Kirrander and Mr D Bellshaw for many helpful discussions.

Supplementary Material

Crystal structures and structural optimization criteria; CRYSTAL17 computational methods; phonon calculations; analysis of N-N interactions in crystalline azides (COHP); identification of target frequencies; anharmonic mode coupling in LiN_3; integration window effect; integration of multi-phonon density of states.

REFERENCES

(1) Klapötke, T. M. *Chemistry of High-Energy Materials*, 2nd ed.; De Gruyter: Berlin, 2012.

(2) Matyáš, R.; Pachman, J. *Primary Explosives*; Springer-Verlag: Berlin, 2013.

(3) Millar, D. I. A.; Oswald, I. D. H.; Francis, D. J.; Marshall, W. G.; Pulham, C. R.; Cumming, A. S. The Crystal Structure of Beta-RDX-an Elusive Form of an Explosive Revealed. *Chem. Commun.* **2009**, No. 5, 562–564.

(4) Millar, D. I. A.; Oswald, I. D. H.; Barry, C.; Francis, D. J.; Marshall, W. G.; Pulham, C. R.; Cumming, A. S. Pressure-Cooking of Explosives—the Crystal Structure of ε-RDX as Determined by X-Ray and Neutron Diffraction. *Chem. Commun.* **2010**, *46* (31), 5662–5664.

(5) Dreger, Z. A. Energetic Materials under High Pressures and Temperatures : Stability , Polymorphism and Decomposition of RDX. *J. Phys. Conf. Ser* **2012**, *377*, 012047.

(6) Bolton, O.; Matzger, A. J. Improved Stability and Smart-Material Functionality Realized in an Energetic Cocrystal. *Angew. Chemie - Int. Ed.* **2011**, *50* (38), 8960–8963.

(7) Landenberger, K. B.; Bolton, O.; Matzger, A. J. Energetic-Energetic Cocrystals of Diacetone Diperoxide (DADP): Dramatic and Divergent Sensitivity Modifications via Cocrystallization. *J. Am. Chem. Soc.* **2015**, *137* (15), 5074–5079.

(8) Zhang, J.; Shreeve, J. M. Time for Pairing: Cocrystals as Advanced Energetic Materials. *CrystEngComm* **2016**, *18* (33), 6124–6133.

(9) Aakeröy, C. B.; Wijethunga, T. K.; Desper, J. Crystal Engineering of Energetic Materials: Co-Crystals of Ethylenedinitramine (EDNA) with Modified Performance and Improved Chemical Stability. *Chem. - A Eur. J.* **2015**, *21* (31), 11029–11037.

(10) Yan, Q.-L.; Zeman, S. Theoretical Evaluation of Sensitivity and Thermal Stability for High Explosives Based on Quantum Chemistry Methods: A Brief Review. *Int. J. Quantum Chem.* **2013**, *113* (8), 1049–1061.

(11) Zeman, S.; JungovÃ¡, M. Sensitivity and Performance of Energetic Materials. *Propellants, Explos. Pyrotech.* **2016**, *41* (3), 426–451.

(12) Tsyshevsky, R. V.; Sharia, O.; Kuklja, M. M. Molecular Theory of Detonation Initiation: Insight from First Principles Modeling of the Decomposition Mechanisms of Organic Nitro Energetic Materials. *Molecules* **2016**, *21* (2).

(13) Mathieu, D. Sensitivity of Energetic Materials: Theoretical Relationships to Detonation Performance and Molecular Structure. *Ind. Eng. Chem. Res.* **2017**, *56* (29), 8191–8201.

(14) Badders, N. R.; Wei, C.; Aldeeb, A. A.; Rogers, W. J.; Mannan, M. S. Predicting the Impact Sensitivities of Polynitro Compounds Using Quantum Chemical Descriptors. *J. Energ. Mater.* **2006**, *24* (1), 17–33.

(15) *Energetic Materials*, 1st ed.; Politzer, P., Murray, J. S., Eds.; Elsevier: Amsterdam, 2003; Vol. 12.

(16) Kamlet, M. J.; Adolph, H. G. The Relationship

of Impact Sensitivity with Structure of Organic High Explosives. II. Polynitroaromatic Explosives. *Propellants, Explos. Pyrotech.* **1979**, *4* (2), 30–34.

(17) Politzer, P.; Murray, J. S. Relationships between Dissociation Energies and Electrostatic Potentials of C-NO2 Bonds: Applications to Impact Sensitivities. *J. Mol. Struct.* **1996**, *376* (1–3), 419–424.

(18) Murray, J. S.; Lane, P.; Politzer, P. Relationships between Impact Sensitivities and Molecular Surface Electrostatic Potentials of Nitroaramatic and Nitroheterocyclic Molecules. *Mol. Phys.* **1995**, *85* (1), 1–8.

(19) Cartwright, M.; Wilkinson, J. Correlation of Structure and Sensitivity in Inorganic Azides i Effect of Non-Bonded Nitrogen Nitrogen Distances. *Propellants, Explos. Pyrotech.* **2010**, *35* (4), 326–332.

(20) Li, J. Relationships for the Impact Sensitivities of Energetic C-Nitro Compounds Based on Bond Dissociation Energy. *J. Phys. Chem. B* **2010**, *114* (6), 2198–2202.

(21) Rice, B. M.; Sahu, S.; Owens, F. J. Density Functional Calculations of Bond Dissociation Energies for NO 2 Scission in Some Nitroaromatic Molecules. *J. Mol. Struct. THEOCHEM* **2002**, *583* (1), 69–72.

(22) Mathieu, D.; Alaime, T. Predicting Impact Sensitivities of Nitro Compounds on the Basis of a Semi-Empirical Rate Constant. *J. Phys. Chem. A* **2014**, *118* (41), 9720–9726.

(23) Asay, B. W.; Henson, B. F.; Smilowitz, L. B.; Dickson, P. M. On the Difference in Impact Sensitivity of Beta and Delta Hmx. *J. Energ. Mater.* **2003**, *21* (4), 223–235.

(24) Bondarchuk, S. V. Impact Sensitivity of Crystalline Phenyl Diazonium Salts: A First-Principles Study of Solid-State Properties Determining the Phenomenon. *Int. J. Quantum Chem.* **2017**, *117* (21).

(25) Ma, Y.; Zhang, A.; Zhang, C.; Jiang, D.; Zhu, Y.; Zhang, C. Crystal Packing of Low-Sensitivity and High-Energy Explosives. *Cryst. Growth Des.* **2014**, *14* (9), 4703–4713.

(26) Zhang, J.; Zhang, Q.; Vo, T. T.; Parrish, D. A.; Shreeve, J. M. Energetic Salts with Stacking and Hydrogen-Bonding Interactions Lead the Way to Future Energetic Materials. *J. Am. Chem. Soc.* **2015**, *137* (4), 1697–1704.

(27) Lewis, J. P.; Sewell, T. D.; Evans, R. B.; Voth, G. A. Electronic Structure Calculation of the Structures and Energies of the Three Pure Polymorphic Forms of Crystalline HMX. *J. Phys. Chem. B* **2000**, *104* (5), 1009–1013.

(28) Politzer, P.; Murray, J. S. Impact Sensitivity and Crystal Lattice Compressibility/Free Space. *J. Mol. Model.* **2014**, *20* (5).

(29) Pospisil, M.; Vavra, P.; Concha, M. C.; Murray, J. S.; Politzer, P. A Possible Crystal Volume Factor in the Impact Sensitivities of Some Energetic Compounds. *J. Mol. Model.* **2010**, *16* (5), 895–901.

(30) Zhu, W.; Xiao, H. Ab Initio Study of Electronic Structure and Optical Properties of Heavy Metal Azides: TlN3, AgN3 and CuN3. *J. Comput. Chem.* **2007**, *29* (2), 176–184.

(31) Zhu, W.; Xiao, H. First-Principles Band Gap Criterion for Impact Sensitivity of Energetic Crystals: A Review. *Struct. Chem.* **2010**, *21* (3), 657–665.

(32) Bondarchuk, S. V. Quantification of Impact Sensitivity Based on Solid-State Derived Criteria. *J. Phys. Chem. A* **2018**, *122*, 5455–5463.

(33) Keshavarz, M. H.; Zali, A.; Shokrolahi, A. A Simple Approach for Predicting Impact Sensitivity of Polynitroheteroarenes. *J. Hazard. Mater.* **2009**, *166* (2–3), 1115–1119.

(34) McGrane, S. D.; Barber, J.; Quenneville, J. Anharmonic Vibrational Properties of Explosives from Temperature-Dependent Raman. *J. Phys. Chem. A* **2005**, *109* (44), 9919–9927.

(35) Piryatinski, A.; Tretiak, S.; Sewell, T. D.; McGrane, S. D. Vibrational Spectroscopy of Polyatomic Materials: Semiempirical Calculations of Anharmonic Couplings and Infrared and Raman Linewidths in Naphthalene and PETN Crystals. *Phys. Rev. B - Condens. Matter Mater. Phys.* **2007**, *75* (21), 1–9.

(36) Ye; Koshi, M. Theoretical Studies of Energy Transfer Rates of Secondary Explosives. *J. Phys. Chem. B* **2006**, *110* (37), 18515–18520.

(37) McNesby, K. L.; Coffey, C. S. Spectroscopic Determination of Impact Sensitivities of Explosives. *J. Phys. Chem. B* **1997**, *101* (16), 3097–3104.

(38) Fried, L. E.; Ruggiero, a J. Energy-Transfer Rates in Primary, Secondary, and Insensitive Explosives. *J. Phys. Chem.* **1994**, *98* (39), 9786–9791.

(39) Bernstein, J. *Ab Initio* Study of Energy Transfer Rates and Impact Sensitivities of Crystalline Explosives. *J. Chem. Phys.* **2018**, *148* (8), 084502.

(40) Dlott, D. D.; Fayer, M. D. Shocked Molecular Solids: Vibrational up Pumping, Defect Hot Spot Formation, and the Onset of Chemistry. *J.*

Chem. Phys. **1990**, *92* (6), 3798–3812.

(41) Tokmakoff, A.; Fayer, M. D.; Dlott, D. D. Chemical Reaction Initiation and Hot-Spot Formation in Shocked Energetic Molecular Materials. *J. Phys. Chem.* **1993**, *97* (9), 1901–1913.

(42) Millar, D. I. A.; Barry, C.; Marshall, W. G.; Pulham, C. R. Structural Characterization of Sodium Azide and Sodium Bifluoride at High Pressures. *Zeitschrift fur Krist.* **2014**, *229* (3), 259–275.

(43) Medvedev, S. A.; Eremets, M. I.; Evers, J.; Klapötke, T. M.; Palasyuk, T.; Trojan, I. A. Pressure Induced Polymorphism in Ammonium Azide (NH 4 N 3). *Chem. Phys.* **2011**, *386* (1–3), 41–44.

(44) Bowden, F. P.; Williams, H. T. Initiation and Propagation of Explosion in Azides and Fulminates. *Proc. R. Soc. London. Ser. A Math. Phys. Sci.* **1951**, *208* (1093), 176–188.

(45) Campbell, R.; Konar, S.; Hunter, S.; Pulham, C.; Portius, P. Labile Low-Valent Tin Azides: Syntheses, Structural Characterization, and Thermal Properties. *Inorg. Chem.* **2018**, *57*, 400–411.

(46) Gray, P.; Waddington, T. . Fundamental Vibration Frequencies and Force Constants in the Azide Ion. *Trans. Faraday Soc.* **1957**, *53*, 901–908.

(47) Fox, P. G. The Explosive Sensitivity of the Metal Azides to Impact. *J. Solid State Chem.* **1970**, *2* (4), 491–502.

(48) John, E. F. Hot Spot Ignition Mechanisms for Explosives. *Acc. Chem. Res.* **1992**, *25* (11), 489–496.

(49) Heinicke, G. *Tribochemistry*; Akademic-Verlag: Berlin, GDR, 1984.

(50) Dlott, D. D. Ultrafast Vibrational Energy Transfer in the Real World: Laser Ablation, Energetic Solids, and Hemeproteins. *J. Opt. Soc. Am. B* **1990**, *7* (8), 1638.

(51) Zel'dovich, Y. B.; Raizer, Y. P. *Physics of Shock Waves and High-Temperature Hydrodynamic Phenomena*, Vol II, Ch.; Academic: New York, 1967.

(52) Zerilli, F. J.; Toton, E. T. Shock-Induced Molecular Excitation in Solids. *Phys. Rev. B* **1984**, *29* (10), 5891–5902.

(53) Walker, F. E. Physical Kinetics. *J. Appl. Phys.* **1988**, *63* (11), 5548–5554.

(54) Bardo, R. D. Theoretical Calculations of Rate-Determining Steps for Ignition of Shocked, Condensed Nitromethane. *Int. J. Quantum Chem.* **1986**, *30* (20 S), 455–469.

(55) Coffey, C. S.; Toton, E. T. A Microscopic Theory of Compressive Wave-Induced Reactions in Solid Explosives. *J. Chem. Phys.* **1982**, *76* (2), 949–954.

(56) Hill, J. R.; Chronister, E. L.; Chang, T.; Kim, H.; Postlewaite, J. C.; Dlott, D. D. Vibrational Relaxation and Vibrational Cooling in Low Temperature Molecular Crystals. *J. Chem. Phys.* **1988**, *88* (2), 949–967.

(57) Dlott, D. D. Optical Phonon Dynamics in Molecular Crystals. *Ann. Rev. Phys. Chem.* **1986**, *37*, 157–187.

(58) Hooper, J. Vibrational Energy Transfer in Shocked Molecular Crystals. *J. Chem. Phys.* **2010**, *132* (1).

(59) Manaa, M. R. Shear-Induced Metallization of Triamino-Trinitrobenzene Crystals. *Appl. Phys. Lett.* **2003**, *83* (7), 1352–1354.

(60) Kuklja, M. M.; Aduev, B. P.; Aluker, E. D.; Krasheninin, V. I.; Krechetov, A. G.; Mitrofanov, A. Y. Role of Electronic Excitations in Explosive Decomposition of Solids. *J. Appl. Phys.* **2001**, *89* (7), 4156–4166.

(61) Kuklja, M. M.; Rashkeev, S. N. Shear-Strain-Induced Chemical Reactivity of Layered Molecular Crystals. *Appl. Phys. Lett.* **2007**, *90* (15), 2005–2008.

(62) Werner, H. J.; Knowles, P. J.; Knizia, G.; Manby, F. R.; Schütz, M. Molpro: A General-Purpose Quantum Chemistry Program Package. *Wiley Interdiscip. Rev. Comput. Mol. Sci.* **2012**, *2* (2), 242–253.

(63) Giannozzi, P.; Baroni, S.; Bonini, N.; Calandra, M.; Car, R.; Cavazzoni, C.; Ceresoli, D.; Chiarotti, G. L.; Cococcioni, M.; Dabo, I.; et al. QUANTUM ESPRESSO: A Modular and Open-Source Software Project for Quantum Simulations of Materials. *J. Phys. Condens. Matter* **2009**, *21* (39), 395502.

(64) Perdew, J. P.; Burke, K.; Ernzerhof, M. Generalized Gradient Approximation Made Simple. *Phys. Rev. Lett.* **1996**, *77* (18), 3865–3868.

(65) Lücke, A.; Gerstmann, U.; Kühne, T. D.; Schmidt, W. G. Efficient PAW-Based Bond Strength Analysis for Understanding the In/Si(111)(8 × 2) – (4 × 1) Phase Transition. *J. Comput. Chem.* **2017**, *38* (26), 2276–2282.

(66) Dovesi, R.; Orlando, R.; Erba, A.; Zicovich-Wilson, C. M.; Civalleri, B.; Casassa, S.; Maschio, L.; Ferrabone, M.; De La Pierre, M.; D'Arco, P.; et al. CRYSTAL14: A Program for the Ab Initio Investigation of Crystalline Solids. *Int. J. Quantum Chem.* **2014**, *114* (19), 1287–1317.

(67) Krukau, A. V.; Vydrov, O. A.; Izmaylov, A. F.; Scuseria, G. E. Influence of the Exchange Screening Parameter on the Performance of Screened Hybrid Functionals. *J. Chem. Phys.* **2006**, *125* (22).

(68) Garza, A. J.; Scuseria, G. E. Predicting Band Gaps with Hybrid Density Functionals. **2016**, *7*, 5–10.

(69) Clark, S. J.; Segall, M. D.; Pickard, C. J.; Hasnip, P. J.; Probert, M. I. J.; Refson, K.; Payne, M. C. First Principles Methods Using CASTEP. *Zeitschrift für Krist.* **2005**, *220*, 567–570.

(70) Refson, K.; Tulip, P. R.; Clark, S. J. Variational Density-Functional Perturbation Theory for Dielectrics and Lattice Dynamics. *Phys. Rev. B - Condens. Matter Mater. Phys.* **2006**, *73* (15), 1–12.

(71) Verneker, V. R. P.; Avrami, L. Explosive Behavior of Barium Azide. *J. Phys. Chem.* **1968**, *72* (3), 778–783.

(72) Marinkas, P. L. A Method of Growing Anhydrous Single Crystals of Barium Azide. *Nature* **1966**, *211*, 1288–1289.

(73) Avrami, L.; Hutchinson, R. The Sensitivity to Impact and Friction. In *Energetic Materials: Technology of the Inorganic Azides*; Fair, H. ., Walker, R. F., Eds.; 1977; pp 111–159.

(74) *Energetic Materials 1: Physics and Chemistry of the Inoganic Azides*; Fair, H. D., Walker, R. F., Eds.; Plenum Press: New York, 1977.

(75) Schulz, A.; Villinger, A. Binary Zinc Azides. *Chem. - A Eur. J.* **2016**, *22* (6), 2032–2038.

(76) Shaneyfelt, W. *Complexities of Lead Azide*; 1984. 21st DDESB Explosives Safety Seminar

(77) Wohler, L.; Martin, F. *New Fulminates and Azides*; 1917. Chemische Berichte

(78) Bresien, J.; Ott, H.; Rosenstengel, K.; Schulz, A.; Thiele, P.; Villinger, A. Binary Polyazides of Zinc. *Eur. J. Inorg. Chem.* **2016**, *2016* (36), 5594–5609.

(79) Yakovleva, G. .; Kurbangalina, R. K.; Stesik, L. N. Detonation Properties of Ammonium Azide. *Combust. Explos. Shock Waves* **1977**, *13*, 405–407.

(80) Denisaev, A. A.; Assovskii, I. G.; Berlin, A. A. A. Study of the Impact Sensitivity of Sodium Azide and Its Mixtures with Water. *Dokl. Phys. Chem.* **2013**, *453* (1), 261–263.

(81) Damse, R. S. Studies on the Decomposition Chemistry of Triaminoguanidine Azide and Guanidine Nitrate. *J. Hazard. Mater.* **2009**, *172* (2–3), 1383–1387.

(82) Evers, J.; Göbel, M.; Krumm, B.; Martin, F.; Medvedyev, S.; Oehlinger, G.; Steemann, F. X.; Troyan, I.; Klapötke, T. M.; Eremets, M. I. Molecular Structure of Hydrazoic Acid with Hydrogen-Bonded Tetramers in Nearly Planar Layers. *J. Am. Chem. Soc.* **2011**, *133* (31), 12100–12105.

(83) Zhang, G.; Weeks, B. L. A Device for Testing Thermal Impact Sensitivity of High Explosives. *Propellants, Explos. Pyrotech.* **2010**, *35* (5), 440–445.

(84) Grechnev, A.; Ahuja, R.; Eriksson, O. Balanced Crystal Orbital Overlap Population - A Tool for Analysing Chemical Bonds in Solids. *J. Phys. Condens. Matter* **2003**, *15* (45), 7751–7761.

(85) Liu, C.; Tranca, I.; Van Santen, R. A.; Hensen, E. J. M.; Pidko, E. A. Scaling Relations for Acidity and Reactivity of Zeolites. *J. Phys. Chem. C* **2017**, *121* (42), 23520–23530.

(86) Deringer, V. L.; Englert, U.; Dronskowski, R. Covalency of Hydrogen Bonds in Solids Revisited. *Chem. Commun.* **2014**, *50* (78), 11547–11549.

(87) Xu, C.; Yu, L.; Zhu, C.; Yu, J.; Cao, Z. Intersystem Crossing-Branched Excited-State Intramolecular Proton Transfer for o-Nitrophenol: An Ab Initio on-the-Fly Nonadiabatic Molecular Dynamic Simulation. *Sci. Rep.* **2016**, *6* (March), 1–12.

(88) Perry, J. K.; Tahir-Kheli, J.; Goddard, W. A. Antiferromagnetic Band Structure of La2CuO4: Becke-3-Lee-Yang-Parr Calcualations. *Phys. Rev. B* **2001**, *63* (14), 144510.

(89) Ramesh Babu, K.; Vaitheeswaran, G. Lattice Dynamics and Electronic Structure of Energetic Solids LiN3and NaN3: A First Principles Study. *Chem. Phys. Lett.* **2013**, *586*, 44–50.

(90) Lindroth, D. O.; Erhart, P. Thermal Transport in van Der Waals Solids from First-Principles Calculations. *Phys. Rev. B* **2016**, *94* (11), 1–11.

(91) Zhang, H.; Cheung, F.; Zhao, F.; Cheng, X. Band Gaps and the Possible Effect on Impact Sensitivity for Some Nitro Aromatic Explosive Materials. *Int. J. Quantum Chem.* **2009**, *109*, 1547–1552.

(92) Winther, K. T.; Thygesen, K. S. Band Structure Engineering in van Der Waals Heterostructures via Dielectric Screening : The G Δ W Method. *2D Mater.* **2017**, *4* (025059).

(93) Balachandran, P. V.; Rondinelli, J. M. Massive Band Gap Variation in Layered Oxides through Cation Ordering. *Nat. Commun.* **2015**, *6*, 1–7.

(94) Paulatto, L.; Mauri, F.; Lazzeri, M. Anharmonic Properties from a Generalized Third-Order Ab Initio Approach: Theory and Applications to

Graphite and Graphene. *Phys. Rev. B - Condens. Matter Mater. Phys.* **2013**, *87* (21), 1–18.

(95) Aynajian, P. *Electron-Phonon Interaction in Conventional and Unconventional Superconductors*; Springer-Verlag: Berlin, 2010.

(96) Bryant, J. I. Vibrational Spectrum of Barium Azide Single Crystals. *J. Chem. Phys.* **1970**, *52*, 4867.

Table of contents graphic